





Research article

# Anti-rust primer for steel based on natural rubber bearing methacrylic functionality

Rattanawadee Ninjan<sup>1</sup>, Bencha Thongnuanchan<sup>1\*</sup>, Natinee Lopattananon<sup>1</sup>,  
Charoen Nakason<sup>2</sup>

<sup>1</sup>Department of Rubber Technology and Polymer Science, Faculty of Science and Technology, Prince of Songkla University, 94000 Pattani, Thailand

<sup>2</sup>Faculty of Science and Industrial Technology, Prince of Songkla University, 84000 Surat Thani, Thailand

Received 11 November 2021; accepted in revised form 9 February 2022

**Abstract.** This study aimed to develop an anti-corrosion primer for steel based on natural rubber (NR). Graft copolymers of NR and poly(methacrylic acid), NR-g-PMAA, were first synthesized using a solution polymerization technique. The degree of grafting of poly(methacrylic acid) in NR-g-PMAA was evaluated by the <sup>1</sup>H-NMR technique. The primer was then prepared by compounding the synthesized NR-g-PMAA with colour pigment and isocyanate crosslinking agent (poly-HDI). The X-ray photoelectron spectroscopy analysis indicated the formation of amide and anhydride linkages in the NR-g-PMAA primer by reaction with poly-HDI under ambient conditions. The cross-cut and salt-spray tests suggested that good adhesion of the primer to the steel was achieved by adding a 2:1 molar ratio of poly-HDI:MAA. The addition of poly-HDI to the NR-g-PMAA primer also significantly improved its weathering resistance. No rust deposits formed on the steel coated with the cured primer after 500 h of exposure in a QUV Accelerated Weathering tester. In contrast, a layer of iron oxide formed over the steel coated with the uncured primer, indicating that it corroded during testing. The X-ray diffraction analyses revealed that the iron oxides formed under the experimental conditions were dominantly lepidocrocite and goethite. Hence, it can be stated that when the NR-g-PMAA primer is formulated in conjunction with an appropriate amount of poly-HDI, it offers the potential to develop an anti-rust primer for steel.

**Keywords:** rubber, coating, primer, corrosion, steel

## 1. Introduction

Rubber primers have been widely used for the protection of steel against corrosion. Rubber primer systems typically require both a good adhesion to the steel surface and an appropriate curing system to improve the mechanical properties of the rubber. It has long been known that the adhesion of rubber primer to polar surfaces of steel can take place via a combination of physical and chemical processes [1]. Therefore, an ideal primer is generally based on polar rubbers (*e.g.*, halogenated rubbers and acrylonitrile-butadiene rubber) [2, 3]. The inherent polarity of these rubbers makes them easier to wet the steel surface

than non-polar rubbers. Although halogenated rubber-based primers generally possess excellent resistance to water and moderate solvent resistance, they tend to decompose at high temperatures, releasing toxic compounds (*e.g.*, hydrogen chloride) [4].

The curing of rubber primer can generally be achieved by adding curing agents. The choice of curing agents for the rubber primer also plays a role in determining its properties. Generally, when a rubber primer is cured, its cohesive strength increases due to forming a continuous network of rubber chains in the primer. An additional benefit of crosslinking a rubber primer can usually be seen in improving its weathering

\*Corresponding author, e-mail: [jjthongnuanchan@hotmail.com](mailto:jjthongnuanchan@hotmail.com)

© BME-PT

resistance. Moreover, if a curing agent for a rubber primer can react chemically with metal oxides on the steel surface during the curing process, chemical bridges between the primer and the steel surface are formed [5]. The formation of this type of reaction (*i.e.*, chemisorption) can promote adhesion between the primer and the substrate.

Isocyanate has been widely used as one of the key components in adhesives and primers for bonding rubber to steel. It has been proposed that isocyanate groups (NCO) can undergo condensation reactions with hydroxides of steel, leading to good adhesion of these compounds to steel [6–8]. These reactions typically lead to urethane-like linkage between the isocyanate moiety and the steel surface [9, 10]. Studies of interfacial interactions between isocyanate and steel are normally be conducted using X-ray photoelectron spectroscopy (XPS) [9, 10].

The primary focus of this work is to investigate the feasibility of developing anti-corrosive primers for steel based on natural rubber (NR). However, the proper wetting and coverage of the NR over the steel surface are unlikely to occur as it is a non-polar rubber. Therefore, the application of NR in primer systems has begun from the use of chemically modified NRs. Chlorinated NR has been widely used as anti-corrosion coatings for steel for a long time. It can be prepared by treating a rubber solution with gaseous chlorine or sulfury chloride ( $\text{SO}_2\text{Cl}_2$ ) under suitable conditions [11]. Preparation of chlorinated NR (CNR) in the latex stage has also been reported by Zhong *et al.* [12]. Since the CNR can contain up to approximately 50% by weight of chlorine after the treatment, its polarity and resistance to acids and alkalis increase significantly. However, CNR film is brittle and requires a plasticizer to improve its flexibility for use as a coating [13]. Chlorinated paraffin with a chlorination degree in the range of 30 to 70 wt% is one of the most common plasticizers for CNR. The work of Sakhri *et al.* [14] demonstrated that corrosion started occurring on the steel surface coated with the plasticized CNR primer after immersion in 3.5% NaCl solution for 3 days. Significant improvement in the protective properties of the CNR primer could be achieved by incorporating active pigments (*e.g.*, zinc phosphate and polyaniline pigments).

Epoxidized natural rubber (ENR) is another type of modified NR consisting of oxirane rings along its backbone. The presence of epoxide groups in the ENR molecule makes it chemically reactive. As

reported by Mousaa and Radi [15], corrosion inhibitors for steel were synthesized by reacting ENR with aliphatic amines. A reduction in the corrosion rate for coating systems based on epoxy and urethane acrylate was observed when incorporating these inhibitors at optimum concentrations.

The grafting of polar monomers onto the backbone of the NR can reduce the dissimilarity in polarity between NR and steel, which improves its degree of wetting. Poly(acetoacetoxyethyl methacrylate), PAAEM, was intentionally grafted to the NR backbone to improve its wettability on steel surfaces [16]. This can be because the grafted PAAEM chain contains the acetoacetoxy (AcAc) groups capable of hydrogen bonding with metal hydroxides on the steel surface. In the present study, methacrylic acid was selected for this purpose, and graft copolymers of NR and poly(methacrylic acid), NR-*g*-PMAA, was synthesized via solution polymerization. Poly(methacrylic acid), PMAA, is not only a highly polar polymer, but different crosslinkers can also crosslink the reactive carboxyl groups in its structure.

The synthesis of the NR-*g*-PMAA have been previously reported in the literature [17]. The feasibility of developing a fire-retardant coating for wood based on the NR-*g*-PMAA was demonstrated. The NR-*g*-PMAA was chosen as the base polymer in the corresponding coating as it contained carboxyl groups, which can serve as hydrogen bonding sites. The ability to form hydrogen bonds with hydroxyl groups on the wood surface facilitates the wetting and penetration of the coating into the wood's pores. The paper also provided evidence that NR-*g*-PMAA could be cured by reaction with isocyanurated hexamethylene diisocyanate (poly-HDI) under ambient conditions. However, no significant evidence supported that poly-HDI could react with the hydroxyl groups on the wood surface.

In this work, Poly-HDI was also used as a curing agent for the NR-*g*-PMAA primer. It is expected that the presence of grafted PMAA in the NR molecule enables it to form chemical bonds to the steel surface when using poly-HDI as a crosslinker. Moreover, the carboxyl moiety in the grafted PMAA can also increase the polarity of the NR-based primers, which promotes its adhesion to standard metal paints. The thermal stability of the NR-*g*-PMAA films in the presence and absence of poly-HDI was first investigated using the thermogravimetric analysis (TGA) method. The chemical interactions at the primer/steel

interface were investigated using XPS analysis. The adhesion of the NR-g-PMAA primer on the steel surface was examined using the cross-cut test. The weathering resistance and corrosion test of the primer were studied using a salt spray test and the QUV accelerated weathering tester, respectively.

## 2. Experimental

### 2.1. Materials

The high ammonia concentrated natural rubber (HANR) used in this work was manufactured by Yala Latex Co., Ltd. (Yala, Thailand). The dry rubber content of the HANR latex was 61.4%. The methacrylic acid (MAA) and benzoyl peroxide (BPO) were manufactured by Sigma-Aldrich Chemicals (Steinheim, Germany). An aliphatic poly-HDI with an isocyanate (NCO) content of 25% (w/w), namely Basonat<sup>®</sup> HW 1000, was used as a crosslinking agent in a primer formulation. The poly-HDI was manufactured by BASF SE (Ludwigshafen, Germany). All chemicals were used as received.

### 2.2. A general procedure for the preparation NR-g-PMAA

The synthesis of graft copolymer of NR and PMAA was carried out using the solution polymerization technique. The polymerization was performed at 80 °C under a flowing nitrogen atmosphere. NR (13.5 g) was first masticated on a two-roll mill for 10 min before being dissolved in 85 ml of toluene. The resulting solution was then transferred to a flanged vessel containing MAA monomer (5.8 g) and BPO (0.35 g). The reaction was allowed to proceed for 8 h under stirring.

## 2.3. Characterizations

### 2.3.1. <sup>1</sup>H-NMR characterization

A two-step Soxhlet extraction was performed to purify the crude NR-g-PMAA before structural characterizations. Petroleum ether and acetone were employed as extraction solvents for the ungrafted NR and PMAA homopolymer, respectively.

Each extraction step was conducted for 24 h. The <sup>1</sup>H-NMR spectra of purified NR-g-PMAA were acquired using a Bruker Avance III 400 spectrometer (Bruker BioSpin mbH, Rheinstetten, Germany) in deuterated chloroform (CDCl<sub>3</sub>).

The mol% of the grafted PMAA in the NR-g-PMAA was calculated from the integrated intensity ratio of

the NMR signals at 1.25 ppm and 5.13 ppm, according to the Equation (1):

$$\text{mol\% of PMAA} = \frac{\frac{I_{1.25}}{3}}{\frac{I_{1.25}}{3} + I_{5.13}} \cdot 100 \quad (1)$$

where  $I_{1.25}$  is the integrated peak area of the methyl protons of PMAA in NR-g-PMAA; and  $I_{5.13}$  is the integrated peak area of the olefinic protons of NR. Additionally, the grafting efficiency (GE) of MAA onto the NR molecules can also be estimated from mol% of PMAA in the graft copolymers before and after the extraction, as given in Equation (2) [18]:

$$\text{GE [\%]} = \frac{\text{mol\% of MAA grafted}}{\text{mol\% of total MAA polymerized}} \cdot 100 \quad (2)$$

### 2.3.2. ATR-FTIR characterization

ATR-FTIR analysis was carried out to provide information on functional groups present in the cast films of NR-g-PMAA. The ATR-FTIR spectra of NR-g-PMAA films were collected on a Fourier transform infrared (FTIR) spectrometer (Tensor 27 FTIR spectrometer, Bruker Optics, Ettlingen, Germany) fitted with an ATR accessory. The analysis was recorded between 3500 and 350 cm<sup>-1</sup> at a resolution of 4 cm<sup>-1</sup>.

### 2.3.3. Contact angle

The sessile drop method was used to optically measure contact angles of test liquids (*i.e.*, water and ethylene glycol) on two surfaces of NR and NR-g-PMAA. The measurements were performed using a contact angle meter (DM300, Kyoma Interface Science Co., Saitama, Japan) at ambient temperature. The surface free energies (SFEs) of the rubbers were then estimated from their corresponding contact angles using Wu method, as expressed by the Equation (3) and (4) [19, 20]:

$$0.25(1 + \cos \theta_1) \gamma_{L1} = \frac{\gamma_{L1}^d \gamma_S^d}{\gamma_{L1}^d + \gamma_S^d} + \frac{\gamma_{L1}^p \gamma_S^p}{\gamma_{L1}^p + \gamma_S^p} \quad (3)$$

$$0.25(1 + \cos \theta_2) \gamma_{L2} = \frac{\gamma_{L2}^d \gamma_S^d}{\gamma_{L2}^d + \gamma_S^d} + \frac{\gamma_{L2}^p \gamma_S^p}{\gamma_{L2}^p + \gamma_S^p} \quad (4)$$

where  $\gamma_{L1}$ ,  $\gamma_{L1}^d$  and  $\gamma_{L1}^p$  represent the surface tension, dispersive component and polar component for liquid 1, respectively.  $\theta_1$  is the contact angle of liquid 1.  $\gamma_{L2}$ ,  $\gamma_{L2}^d$  and  $\gamma_{L2}^p$  represent the surface tension, dispersive component and polar component for liquid 2,

respectively.  $\theta_2$  is the contact angle of liquid 2. It is important to note that the value of dispersive component for water and ethylene glycol are 26.0 and 29.0 mN/m, respectively and the value of polar component for water and ethylene glycol are 46.8 and 19.0 mN/m, respectively.

#### 2.3.4. XPS analysis

XPS measurements were conducted using a Kratos AXIS Ultra DLD (Kratos Analytical, Manchester, UK). The measurements were run in the hybrid mode using monochromatic Al-K $\alpha$  radiation (1486.6 eV). The survey spectra were acquired using pass energy of 80 eV at steps sizes of 1000 meV, while high-resolution spectra were collected using pass energy of 160 eV at step sizes of 100 meV. Peak fitting was carried out using Kratos Vision 2 software.

#### 2.3.5. Thermogravimetric analysis

The thermal stability of the NR-g-PMAA films formed in the presence of different levels of poly-HDI was investigated by using the thermogravimetric analysis (TGA) method. TGA was performed using a thermogravimetric analyzer (TGA8000, Perkin-Elmer Inc., Waltham, USA). The analysis was carried out under a nitrogen atmosphere from ambient temperature to 800 °C at the heating rate of 10 °C/min. About 5 mg of the sample was used for each test.

#### 2.3.6. Cross-cut test

The cross-cut test was conducted to determine the adhesion of the NR-g-PMAA primer to the steel surface, according to ASTM D3359-09. Levels of adhesion were classified based on the percentage of primer removed from the steel surface in the cross-cut test. Adhesion was ranked on a scale of 0B-5B. The scale 5B represented relatively perfect adhesion in which no detachment of primer in the cross-cut area was observed after the testing. When more than 65% of the cross-cut area was detached, the scale 0B was given.

#### 2.3.7. Salt spray test

Anti-corrosion resistance of the primer was tested using a salt-spray test (Q-FOG cyclic corrosion tester, Q-Lab Corporation, Westlake, OH, USA) following ASTM B117. The intersection of two scribe lines with a 1 mm width was made in the steel coated with the primer until the underlying steel substrate

was revealed. This testing involved continuous exposure of the coated sample to salt spray (fog) at 35 °C using a 5% sodium chloride solution with a pH ~7.2. The test duration was set to 500 h, and the assessment of the primer damage was done visually.

#### 2.3.8. QUV Weathering test

The weathering test of the primer was conducted on a QUV unit (model QUV/spray, Q Q-Lab Corporation, Westlake, OH, USA). It was programmed to produce cycles of wetness alternating with UV according to ASTM G-53: (a) UVA bulb (340 nm) UV irradiance at 0.68 W/m<sup>2</sup>, 60 °C for 4 h, and (b) condensation at 50 °C for 4 h. The primer was exposed to weathering cycles for 250 and 500 h before its weathering performance was determined.

#### 2.3.9. Scanning electron microscopy

The surface morphologies of the oxide layers formed on the weathering steel were investigated using scanning electron microscope (Quanta 400, Thermo Fisher Scientific, Erlangen, Germany) equipped with an energy dispersive X-ray (EDX) detector (X-Ray Spectrometer EDX, Oxford Instruments, Buckinghamshire, UK). EDX analysis was performed to determine the chemical compositions of the corrosion products.

#### 2.3.10. X-ray diffraction analysis

The crystal structures of corrosion products formed on weathering steels were examined by the X-ray diffraction (XRD) analysis. The XRD analysis was performed using an X-ray diffractometer (Empyrean, PANalytical, Almelo, Netherlands) with a Cu-K $\alpha$  tube ( $\lambda = 0.154$  nm) operated at 40 kV and a current of 30 mA. The diffraction patterns were scanned in the  $2\theta$  range of 5–90° with a step size of 0.026° and time/step of 70.125 sec.

#### 2.3.11. Estimation of the average molecular weight between crosslinks, $M_c$

The equilibrium swelling method was used to estimate the  $M_c$  of the NR-g-PMAA films formed in the presence of different levels of poly-HDI crosslinker. The films were allowed to cure under ambient conditions for 7 days before being analyzed. The crosslinked films were first cut into a circular shape, weighed, and then immersed in toluene until equilibrium was attained. After that, the amount of toluene absorbed by the crosslinked film was determined.



This allowed the determination of the volume fraction of rubber in the swollen network ( $V_r$ ) using the method of Ellis and Welding (Equation (5)) [21]:

$$V_r = \frac{\frac{D-FT}{\rho_r}}{\frac{D-FT}{\rho_r} + \frac{A_s}{\rho_s}} \quad (5)$$

where  $D$  is the deswollen weight of crosslinked film,  $F$  is the volume fraction of the insoluble components (*i.e.*, other than the rubber) in the film,  $T$  is the initial weight of the film.  $A_s$  is the weight of toluene absorbed in the swollen film.  $\rho_r$  and  $\rho_s$  are the densities of rubber and toluene ( $0.865 \text{ g/cm}^3$ ), respectively. The estimation of  $M_c$  from the value of  $V_r$  can be achieved using the well-known Flory-Rehner equation (Equation (6)) [22–24]:

$$M_c = -\frac{\rho_r V_s \left(1 - \frac{2}{f}\right) V_r^{\frac{1}{3}}}{\ln(1 - V_r) + V_r + \chi V_r^2} \quad (6)$$

where  $V_s$  is the molar volume of solvent (toluene =  $106.28 \text{ cm}^3/\text{mol}$ ) and  $\chi$  is the interaction parameter for a specific polymer-solvent pair. It is essential to mention that the value of  $\chi$  for NR-toluene system (0.38) was used in this calculation.  $f$  represents the number of branches originating from a crosslinking site, which is assumed to be tetra-functional networks (*i.e.*,  $f = 4$ ) in this estimation.

The  $M_c$  can also be expressed as crosslink density ( $\nu$ ) where  $\nu = 1/2 \cdot M_c$  in moles of crosslinks per gram of rubber. However, the estimated values for both  $M_c$  and  $\nu$  should be termed apparent  $M_c$  ( $M_{c \text{ app}}$ ) and apparent  $\nu$  ( $\nu_{\text{app}}$ ), respectively, due to uncertainty in the interaction parameter values ( $\chi$ ) for the NR-g-PMAA-toluene system.

#### 2.4. Preparation of NR-g-PMAA primer

The primer was first prepared by mechanical mixing the solution of NR-g-PMAA in toluene (100 g) with red pigment (50 g, 70 phr) for 30 min. After that, poly-HDI crosslinker was mixed into the formulated NR-g-PMAA primer by stirring for 5 min before applying on the steel surface. It is important to note that the pot life of the NR-g-PMAA primer mixed with poly-HDI is about 3 h in an airtight container at room temperature.

The amount of poly-HDI used in each primer formulation was calculated based on the initial moles of MAA present in the grafting reactions, as shown

**Table 1.** Formulations of NR-g-PMAA primers and the estimated values of rubber volume fraction ( $V_r$ ), apparent crosslink density ( $\nu_{\text{app}}$ ) and apparent average molecular weight between crosslinks ( $M_{c \text{ app}}$ ) for the cured primers.

Ingredients	Molar ratio of poly-HDI:MAA		
	0:1	1:1	2:1
NR-g-PMAA compound (34.6% TSC) [g]	20.96	20.78	20.83
Poly-HDI [g]	–	3.91	7.55
<b>Parameters</b>			
Amount of MAA in primer [mmol]	15.98	15.84	15.87
Amount of added poly-HDI [mmol]	–	15.96	30.56
Calculated molar ratio of poly-HDI:MAA [–]	–	1.01:1	1.92:1
$V_r$	–	0.122	0.132
$\nu_{\text{app}}$ [mol/cm <sup>3</sup> ]	–	$4.86 \cdot 10^{-5}$	$5.61 \cdot 10^{-5}$
$M_{c \text{ app}}$ [g/mol]	–	10292	8920

in Table 1. It is important to note that the equivalent weight of isocyanates (NCO) of the poly-HDI is about 247 g. This NCO equivalent weight indicates the amount of poly-HDI as supplied that contains 1 mole of active NCO.

#### 2.5. Preparation of the NR-g-PMAA primer-coated steel

The surface of the steel plate was first subjected to sandblasting to remove surface contaminants (*e.g.*, rust, existing coating, and dirt). After that, it was cleaned with toluene and dried prior to the primer application. In the present study, the primer thickness was controlled by the weight of the primer per unit surface area. About 2 g of NR-g-PMAA-based primer was then brush-coated on a  $7.6 \times 15.2 \text{ cm}^2$  surface of the steel plate. The primer-coated steel was allowed to dry at room temperature for 7 days before it was subjected to testing. After drying, the primer thickness was in the range of 180–200  $\mu\text{m}$ , as measured based on SEM images when the primer was coated with a coating weight of  $\sim 172 \text{ g/m}^2$ .

### 3. Results and discussion

#### 3.1. <sup>1</sup>H-NMR characterization and contact angle

The synthesized graft copolymers are composed of three major components: ungrafted NR, homopolymer of poly(methacrylic acid), and NR-g-PMAA. Thus, the first two components need to be removed

from the crude NR-g-PMAA before the mole percentage [mol%] of grafted PMAA in the NR-g-PMAA can be estimated from its  $^1\text{H-NMR}$  spectra. Figure 1 shows  $^1\text{H-NMR}$  spectra for the crude and purified NR-g-PMAA, prepared using a NR/MAA weight ratio of 70/30. Three characteristic peaks for NR appeared at 1.66, 2.10 and 5.13 ppm, which corresponded to methyl, methylene and olefinic protons in the *cis*-1,4-polyisoprene unit, respectively [25]. The grafting of poly(methacrylic acid), PMAA, onto the NR molecule was confirmed by the appearance of signals at about 1.25 and 1.58 ppm [17]. These signals were assigned to the methyl and methylene protons in the grafted PMAA chains, respectively. It was found that the amount of grafted PMAA in the NR-g-PMAA30 was 18.59 mol%, calculated according to Equation (1). The GE was 66.18% when 30 wt% of MAA was employed in the grafting reaction. In addition, it was also observed that the grafting of PMAA chains onto the NR backbone also affected its polarity. The measurement of water contact angle (WCA) formed on the NR surface allows the characterization of its surface polarity. An increase in surface polarity would improve the wettability of water on a surface, resulting in a reduction in WCA. The WCA on a solid surface depends mainly on the competition between cohesive forces within water molecules and adhesive forces that result

from the interactions between water and substrate molecules [26].

The results reveal that the WCA values for the NR and NR-g-PMAA were 96.1 and 80.3°, respectively. A high value of WCA for NR suggests that water molecules interact to a greater extent with themselves than NR molecules. It leads to poor wetting since water forms a spherical cap on the NR surface with a contact angle greater than 90°.

The WCA tends typically to decrease when the interactions between the water and substrate molecules increase. The adhesive forces between water and the substrate induce the spreading of water on the solid surface [27]. As the WCA value for NR-g-PMAA (80.3°) was less than 90°, it suggests that water has a stronger affinity for the NR-g-PMAA than the NR. This can be because the NR-g-PMAA bears carboxyl groups capable of hydrogen bonding with water.

This observation is consistent with the finding that the WCA increased slightly after the NR-g-PMAA (82.3°) was crosslinked using a 1:1 molar ratio of poly-HDI:MAA. The crosslinking in this system is believed to occur through chemical reactions between the carboxyl groups of NR-g-PMAA and poly-HDI crosslinker. Thus, the quantity of the carboxyl groups exposed on the NR-g-PMAA surface is expected to decrease after the crosslinking reaction, increasing the water contact angle.

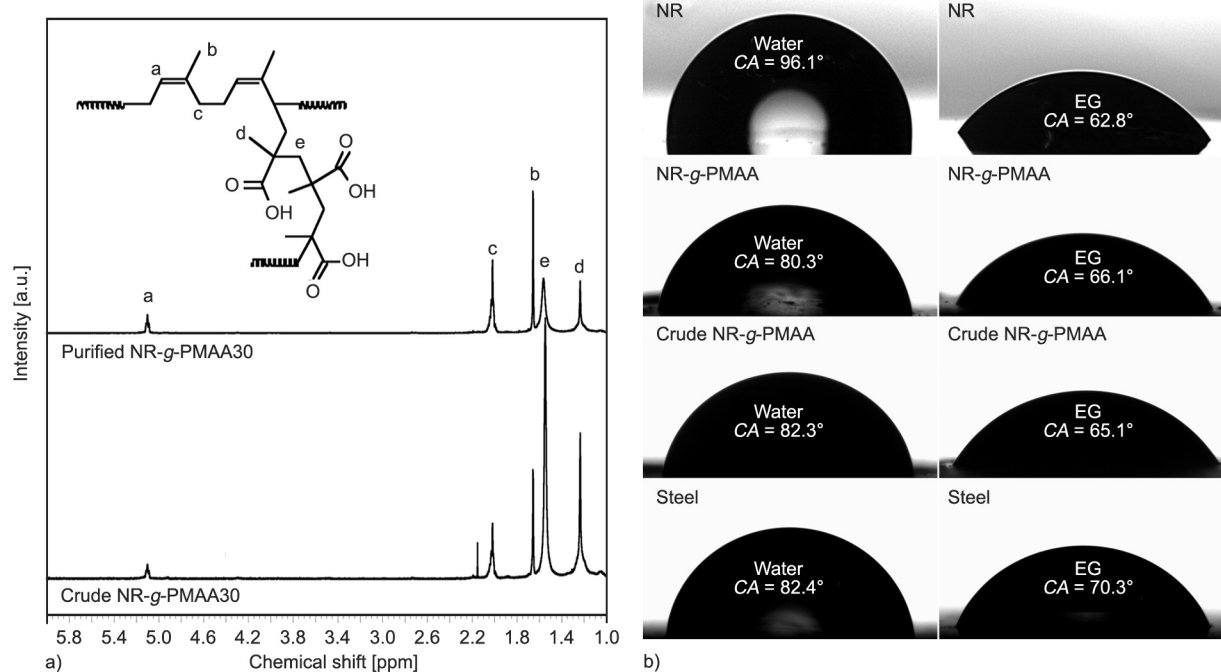


**Figure 1.** (a)  $^1\text{H-NMR}$  spectra of the crude and purified NR-g-PMAA prepared using an initial 30 wt% of MAA along with its structural assignments and (b) contact angle (CA) of water and ethylene glycol (EG) on NR, NR-g-PMAA, cured NR-g-PMAA, and steel.

When ethylene glycol (EG) was used as a test liquid, the contact angles for NR and NR-g-PMAA30 were 62.8 and 66.1°, respectively. A contact angle of ~65.1° was observed for the crosslinked NR-g-PMAA. EG was less polar than water as its polar component of surface free energy (21.3 mN/m) was much lower than that of water (46.8 mN/m). Consequently, the wettability of the NR surface by EG is better than that observed for water.

Water and EG made contact angles of 82.4 and 70.3° with a steel surface that had been sandblasted, respectively (see Figure 1b). The primary reason for applying sandblasting treatment was to remove mill scale and rust from the steel surface before applying the NR-g-PMAA coating. Additionally, the sandblasting process also gave surface roughness to the steel. It is well accepted that the wettability of a liquid droplet on a steel surface is affected by a change in its surface roughness. The influence of roughness on contact angles formed on solid surfaces can be described using a roughness factor ( $r$ ) as given by Wenzel's equation, see Equation (7). Here,  $r$  can be defined as the ratio of the actual surface area ( $A_{\text{smooth}}$ ) to the geometrical area of a surface ( $A_{\text{rough}}$ ), as shown in Equation (8). The value of  $r$  is always greater than unity [28, 29]:

$$\cos \theta_{\text{rough}} = r \cos \theta_{\text{smooth}} \quad (7)$$

$$r = \frac{A_{\text{smooth}}}{A_{\text{rough}}} \quad (8)$$

where  $\theta_{\text{smooth}}$  is the contact angle for the perfectly flat surface, and  $\theta_{\text{rough}}$  represents the apparent contact angles formed on the rough surfaces.

Wenzel's equation suggests that if  $\theta_{\text{smooth}}$  is less than 90°, the roughness will decrease the apparent contact angle. In this case, sandblasting of the steel surface is expected to increase the tendency of a liquid to spread on its surface ( $\theta_{\text{rough}} < \theta_{\text{smooth}}$ ). In contrast, when a surface is hydrophobic ( $\theta_{\text{smooth}} > 90^\circ$ ), the apparent contact angle can be increased by roughening the surface ( $\theta_{\text{rough}} > \theta_{\text{smooth}}$ ). It is essential to mention that Wenzel's equation assumes that there is no effect of roughening on the atomic arrangement of a steel surface. Moreover, it is also assumed that a drop of liquid can wet a rough steel surface without entrapping air thoroughly.

In addition, there is another possible wetting state where a liquid does not wet rough surfaces entirely.

As the surface becomes very rough, it becomes difficult for a liquid to seep between the irregularity of a rough surface. Air can be trapped inside the rough valleys, preventing a liquid droplet from wetting the surface thoroughly. Consequently, a liquid droplet tends to rest on the rough surfaces filled with air instead of completely penetrating the valleys.

This wetting state can be described using the Cassie-Baxter equation [29, 30]. It is proposed that  $\theta_{\text{rough}}$  is related to the area fraction of solid surface under the droplet which is wetted by the liquid ( $f_1$ ) as Equation (9):

$$\cos \theta_{\text{rough}} = r f_1 \cos \theta_{\text{smooth}} - f_2 \quad (9)$$

where  $r$  is the roughness factor and  $f_2$  is the unwetted surface area. Equation (9) demonstrates that the presence of void spaces ( $f_2$ ) increases the apparent contact angle ( $\theta_{\text{rough}} > \theta_{\text{smooth}}$ ).

Therefore, the values of contact angles for the sandblasted steel should be termed the apparent contact angle. As the SFE for steel was also estimated using the measured contact angles, it should also be termed the apparent SFE ( $\text{SFE}_{\text{app}}$ ) due to the uncertainty of absolute values of contact angles.

Changes in polarity of NR after grafting with PMAA can also be evident in an increase in the polar component for the surface free energy (SFE) from 1.83 to 4.68 mN/m. The values of SFE for NR and NR-g-PMAA were 39.15 and 42.01 mN/m, respectively, which was lower than the  $\text{SFE}_{\text{app}}$  of steel (49.78 mN/m).

In addition, the ratio of  $\gamma_s^p/\gamma_s$  for the corresponding surfaces can be used as an indicator of their surface polarities [19, 20]. It was observed that the steel surface was much more polar than both types of the rubbers. This is because the apparent  $\gamma_s^p/\gamma_s$  ratios for the steel (0.122) were higher than those of NR (0.046) and NR-g-PMAA (0.111). These results also indicated that the NR-g-PMAA was more polar than the unmodified NR as it had a higher value of the  $\gamma_s^p/\gamma_s$  ratio (see Table 2).

The apparent work of adhesion is another helpful predictor of adhesion between two contacting solids. It is related to the amount of work required to separate an interface between two solid surfaces. The apparent work of adhesion between the two types of rubber and the steel ( $W_{\text{rubber-steel}}$ ) can also be estimated from their values of surface energy [19, 20], using the Equation (10):

**Table 2.** Dispersive and polar components of surface free energies and the work of adhesion between different types of rubbers and the steel.

Materials	Surface free energy			Polarity $\gamma_s^p/\gamma_s$	Work of adhesion [mN/m]
	$\gamma_s$	$\gamma_s^d$	$\gamma_s^p$		
NR	39.15	37.32	1.83	0.046	87.44 <sup>a</sup>
NR-g-PMAA	42.01	37.33	4.68	0.111	91.45 <sup>a</sup>
Steel after sand-blasting	49.78 <sup>a</sup>	43.70 <sup>a</sup>	6.08 <sup>a</sup>	0.122 <sup>a</sup>	–

<sup>a</sup>Apparent values

$$W_{\text{rubber-steel}} = 2(\sqrt{\gamma_{\text{rubber}}^d \gamma_{\text{steel}}^d} + \sqrt{\gamma_{\text{rubber}}^p \gamma_{\text{steel}}^p}) \quad (10)$$

The NR-g-PMAA/steel interface gave a higher value of 91.45 mN/m for the work of adhesion, compared to that observed for the NR/steel interface (87.44 mN/m). A higher apparent value of  $W_{\text{rubber-steel}}$  suggests stronger interfacial adhesion. Therefore, it is expected that the NR-g-PMAA is more likely to create a better degree of interface contact with steel than NR.

### 3.2. ATR-FTIR analysis

The NR-g-PMAA primer was crosslinked by mixing the appropriate amount of poly-HDI to the formulated NR-g-PMAA solution before casting. The amount of poly-HDI used in this experiment was the stoichiometric 1:1 molar ratio of poly-HDI:MAA. The ATR-FTIR spectra of the NR-g-PMAA casting, in the absence and presence of poly-HDI, were given in Figure 2a. It can be seen that, in both cases, the

cast films exhibited the characteristic peak of the *cis*-1,4-polyisoprene at 835  $\text{cm}^{-1}$ , corresponding to the =C–H out of plane bending. The carboxyl groups, (C=O)–OH, in the poly(methacrylic acid), PMAA, gave an absorption peak at 1710  $\text{cm}^{-1}$  [17]. The corresponding peak was also observed in the FTIR spectra of NR-g-PMAA, which confirmed the grafting of PMAA on the NR molecules.

The crosslinking in the primer is thought to mainly occur between the carboxyl groups of the NR-g-PMAA and the isocyanate (NCO) groups of poly-HDI (see Figure 2b). It has been reported that the reactions of isocyanate with aliphatic carboxylic acid can form urea, amide, or the anhydride of the corresponding acid [31]. The reaction pathway depends mainly on the degree of substitution on the  $\alpha$ -carbon of the aliphatic carboxylic acid. The amides tend to be the predominant products when unhindered aliphatic carboxylic acids are employed. The mixed urea-carboxylic anhydride becomes a predominant product for carboxylic acids with  $\alpha$ -carbon substituents. When poly-HDI was mixed into the NR-g-PMAA primer before casting, new absorption peaks were observed at about 1564 and 1100  $\text{cm}^{-1}$ . The peak at 1564  $\text{cm}^{-1}$  was mainly derived from the N–H bending vibration of amide [32]. The peak at 1100  $\text{cm}^{-1}$  could arise from the stretching vibration of –C–O and/or –CO–O–CO– bonds [33].

### 3.3. XPS analysis

XPS survey spectra of the NR-g-PMAA primer, with the addition of poly-HDI are shown in Figure 3a.

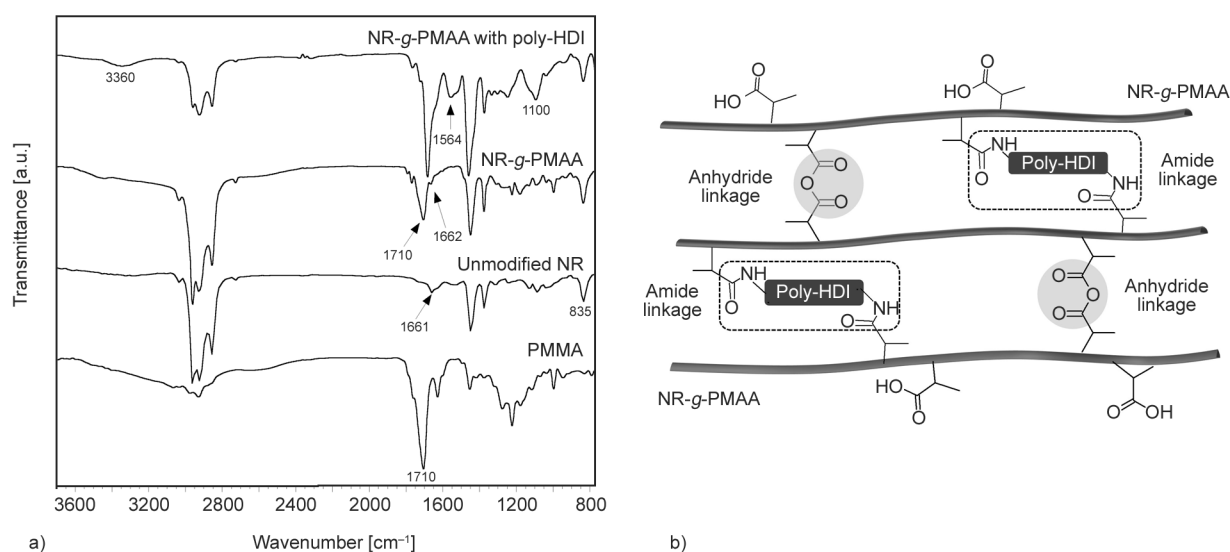


**Figure 2.** (a) An overlay of FTIR spectra for PMAA, NR, and NR-g-PMAA cast films in the presence and absence of poly-HDI and (b) proposed crosslinking reactions between methacrylic functionality in the NR-g-PMAA with poly-HDI.

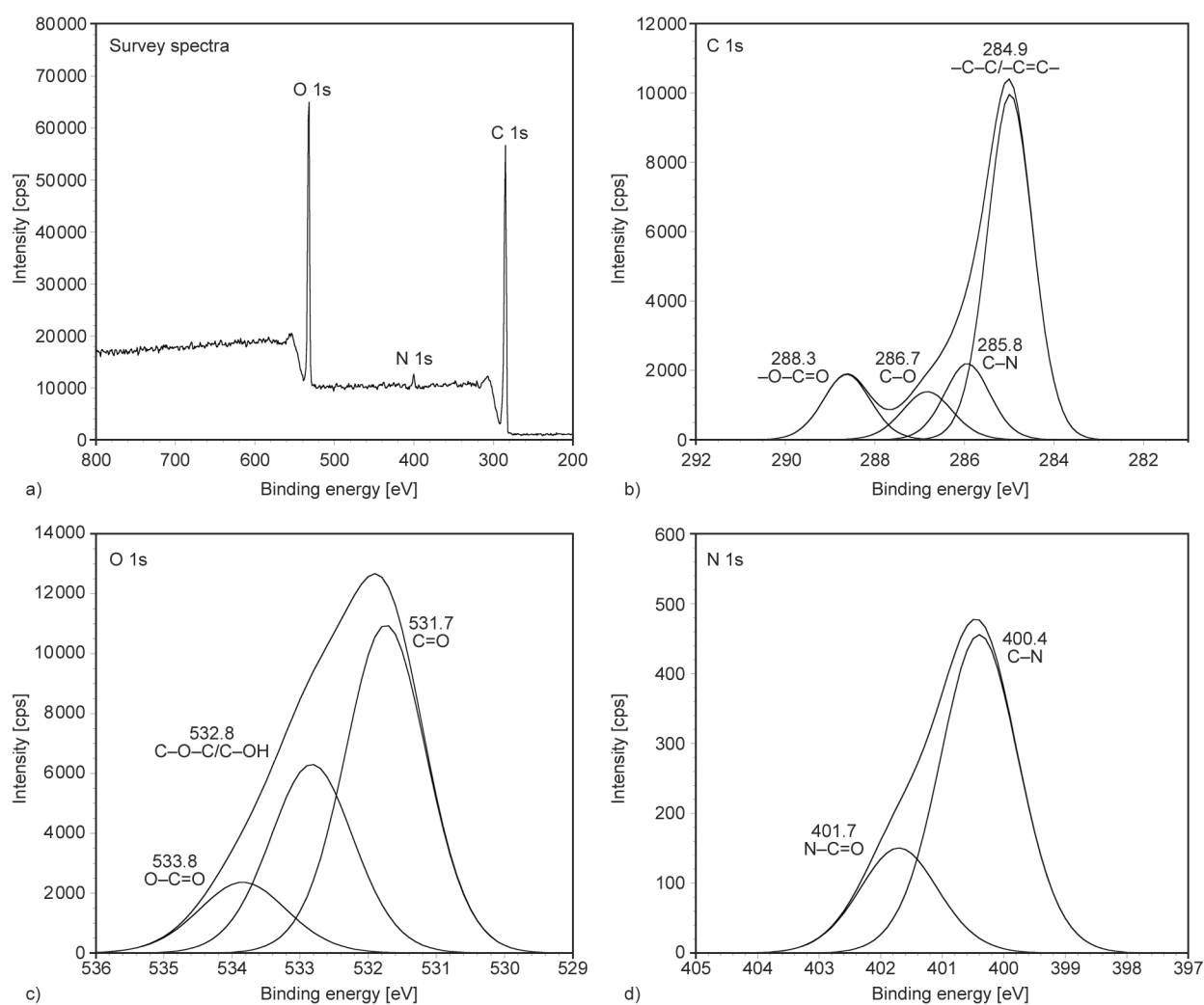


The spectra provided information about the elemental composition of the NR-g-PMAA primer. Carbon (69.13%) and oxygen (28.97%) were the main elements that made up the constituents of the NR-g-PMAA primer. Peaks centred at 284.3 and 531.3 eV were assigned to the C 1s orbital and the O 1s orbital, respectively. It can also be seen that nitrogen (1.90%) was also present on the NR-g-PMAA primer. The N 1s exhibited a weak peak at 400 eV, which originated mainly from the poly-HDI crosslinker in the NR-g-PMAA primer.

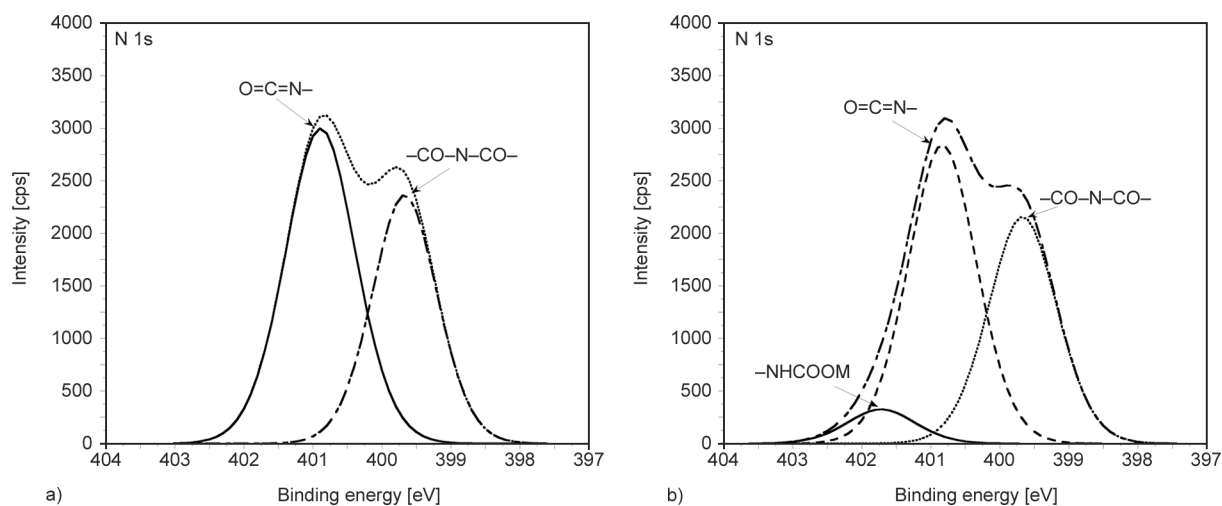
It can be seen from Figure 3b that the C 1s spectra can be deconvoluted into four peaks. The peak at 284.9 eV could be attributed to the  $\underline{\text{C}}-\underline{\text{C}}$  and  $\underline{\text{C}}=\underline{\text{C}}$  bonds [9]. The  $\underline{\text{C}}-\underline{\text{N}}$  and  $\underline{\text{C}}-\underline{\text{O}}$  moieties gave peaks at 285.8 and 286.7 eV, respectively [10]. The peak for the carbon-oxygen double bond ( $\text{O}-\underline{\text{C}}=\text{O}$ ) appeared at 288.3 eV [34].

Figure 3c reveals that three types of oxygen were present in the NR-g-PMAA primer as the O 1s spectra could be deconvoluted into three components. The peak at 531.7 eV was associated with the carbon double bonded to oxygen ( $\text{C}=\underline{\text{O}}$ ), while the peak at 532.8 eV supposed the presence of the  $\text{C}-\underline{\text{O}}-\text{C}$  and  $\text{C}-\underline{\text{O}}-\text{H}$  bond. The peak at 533.8 eV corresponded to oxygen bonded to a carbonyl group ( $\underline{\text{O}}-\text{C}=\text{O}$ ), supporting the existence of anhydride groups [9].

Deconvolution of the N 1s region shows the presence of two main types of N atoms (see Figure 3d). The peaks at 400.4 eV corresponded to the  $\text{C}-\underline{\text{N}}$  [35, 36], which originated mainly from the structure of poly-HDI. The  $\underline{\text{N}}-\text{C}=\text{O}$  peak located at 401.7 eV indicated the presence of the amide functionality [35, 36]. Hence, it can be stated that the XPS finding was corroborated with the FTIR observation. These results provide evidence that the crosslinking reaction



**Figure 3.** (a) The survey XPS spectra and high-resolution spectra of (b) C 1s, (c) O 1s, and (d) N 1s for the NR-g-PMAA primer crosslinked with poly-HDI.



**Figure 4.** High-resolution XPS spectra of N 1s for (a) bulk poly-HDI and (b) a thin film of poly-HDI coated on the steel surface for 7 days under ambient conditions.

of NR-*g*-PMAA with poly-HDI resulted in the formation of both amide and anhydride linkages.

It is also essential to study the interactions occurring at the interfaces to understand better the NR-*g*-PMAA primer's adhesion on the steel surface. XPS was also employed to study the interfacial interactions of the steel with poly-HDI. A thin layer of poly-HDI formed on the steel surface was allowed to cure under ambient conditions for 7 days before being analyzed by XPS. As shown in Figure 4a, the N 1s spectra of the bulk poly-HDI exhibited a broad asymmetric peak, which could be fitted with two components. The peaks at 399.68 and 400.90 eV were assigned to the N atoms in imide (CO-N-CO) and NCO groups, respectively [37].

However, deconvolution of N 1s peak for poly-HDI coated on the steel surface showed the presence of three components (see Figure 4b). The new component was observed on the higher binding energy side of the NCO peak, centred at 401.57 eV. The corresponding peak provides evidence of the chemical reactions occurring at the interface between poly-HDI and NR-*g*-PMAA primer, leading to the formation of urethane-like bonding,  $\text{-HN-CO-OFe}$ , (Fe = steel surface) [9, 10].

The presence of chemical bonds at the poly-HDI/primer interfaces is expected to improve primer adhesion on the steel surface. This is because poly-HDI can crosslink the NR-*g*-PMAA primer and react with the metal hydroxide on the steel surface. Thus, chemical bridges between the primer and steel surface can be formed by reaction with poly-HDI.

### 3.4. TGA analysis

The formation of a crosslinking network in the NR-*g*-PMAA primer can also be reflected by its thermal stability. The thermal degradation behaviors of NR-*g*-PMAA primers in the presence or absence of poly-HDI were determined using TGA under nitrogen atmosphere. TGA curves for the uncured primer and the primer cured with two different levels of poly-HDI: MAA molar ratios are shown in Figure 5.

It can be seen that there were two significant mass loss steps in the decomposition process of the NR-*g*-PMAA primer without the addition of poly-HDI. The first decomposition step began at about 160 °C, corresponding to the peak of the derivative thermogravimetric (DTG) curve at 240 °C (see Figure 5b). The first-step mass loss for the uncured primer is mainly due to the dehydration of carboxyl groups in the NR-*g*-PMAA to give six-membered anhydride rings [38, 39].

The second step for the uncured primer started at about 286 °C, responsible for its significant mass loss (74.7%). This corresponded to the thermal degradation of NR, which was the origin of the DTG peak at 392 °C. However, the shoulder peak could be seen around 427 °C in the DTG curve during the second decomposition step for the uncured primer. The corresponding shoulder peak could be related to the decomposition of the uncured NR-*g*-PMAA phase, which was partially overlapped with the DTG peak for the NR decomposition.

In the case of the cured NR-*g*-PMAA primer, the decomposition process also occurred in two major steps.

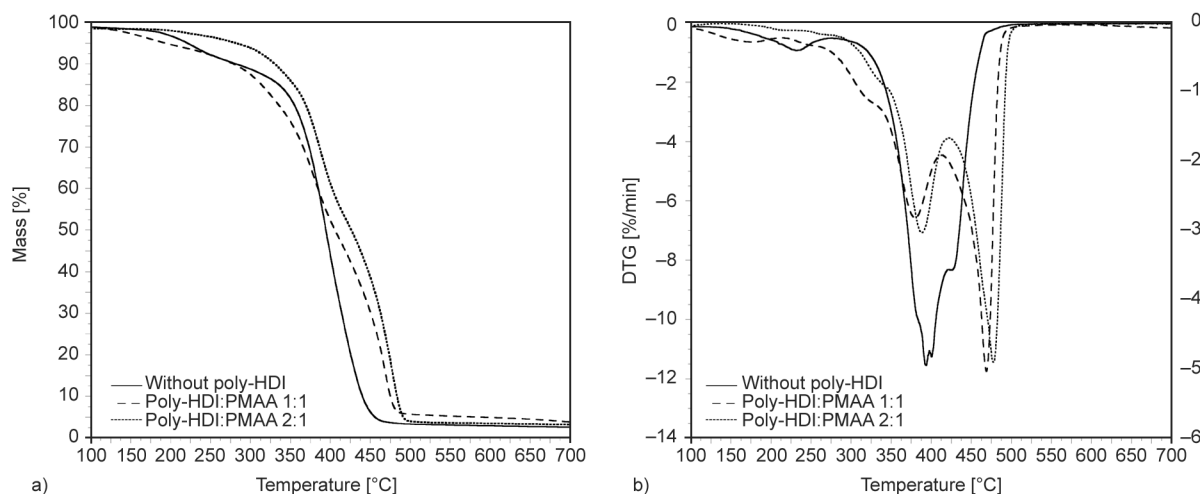


**Figure 5.** (a) TGA thermograms and (b) DTG curves of the NR-g-PMAA primer with addition of different molar ratios of poly-HDI:MAA.

A similar decomposition pattern was observed for the primers cured with 1:1 and 2:1 molar ratios of poly-HDI: MAA. The initial mass loss in the temperature ranges 100–200 °C for the primer cured with a 1:1 molar ratio of poly-HDI:MAA is probably due to the evaporation of volatile contents. The first step of the decomposition for the cured primers exhibited the DTG peaks at 380 and 388 °C, when curing with 1:1 and 2:1 molar ratios of poly-HDI:MAA, respectively. This decomposition step occurred in the temperature range for the thermal degradation of NR (*i.e.*, 300–420 °C) [40].

The second mass loss step for the cured primer was observed between 413 and 530 °C. The cured primer exhibited a mass loss of 44.2 and 42.65% when cured using 1:1 and 2:1 molar ratios of poly-HDI:MAA, respectively. Hence, the mass loss during the second step could be caused by the random-chain scission of the crosslinked NR-g-PMAA chains. Additionally, a shift in the maximum temperature of the DTG peak towards a higher temperature was observed (*i.e.*, from 469 to 478 °C) when the concentration of poly-HDI was increased from 1:1 to 2:1 molar ratio of poly-HDI:MAA. This is attributed to an increase in the level of crosslinking in the primer.

The apparent values of crosslink densities ( $v_{app}$ ) of the cured primer were estimated from equilibrium swelling measurements described by the Flory-Rehner equation. The results in Table 1 reveal that the primer with the addition of two-fold molar excess of poly-HDI ( $v_{app} = 5.61 \cdot 10^{-5} \text{ mol/cm}^3$ ) had higher crosslink density than the primer cured using a stoichiometric amount of poly-HDI ( $v_{app} = 4.86 \cdot 10^{-5} \text{ mol/cm}^3$ ). An increase in the estimated crosslink density was also

accompanied by a reduction of the apparent molecular weight between crosslinks ( $M_{c,app}$ ) in the cured primer (see Table 1).

Moreover, it can also be noticed that there was no peak at about 240 °C in the DTG curve for the primer cured using a two-fold molar excess of poly-HDI. The corresponding DTG peak was caused by the liberation of water from the carboxyl groups in the NR-g-PMAA [41, 42]. Thus, this observation corroborates that the carboxyl groups present in the primers could undergo crosslinking reaction with poly-HDI. As poly-HDI ties carboxyl groups from different chains of NR-g-PMAA into a network, it requires higher thermal energy to induce the thermal breakdown of the crosslinked chains. This increases the thermal stability of the primers with the addition of poly-HDI.

### 3.5. Adhesion test

A cross-cut test was employed to assess the adhesion of the NR-g-PMAA primer to the steel substrate. The steel specimen coated with the NR-g-PMAA primer was allowed to cure at room temperature for 7 days before it was subjected to the testing. Two levels of poly-HDI were used to cure the NR-g-PMAA primer, which corresponded to poly-HDI: MAA molar ratios of 1:1, and 2:1 (see Table 1).

The adhesion of the primer, without the addition of poly-HDI, on the steel surface was first examined, for comparison purposes. It was found that small flakes of the primer in the squares of the lattice were detached, as shown in Figure 6a. However, the detached area was not greater than 35% of the lattice so that the adhesion of the primer without poly-HDI was



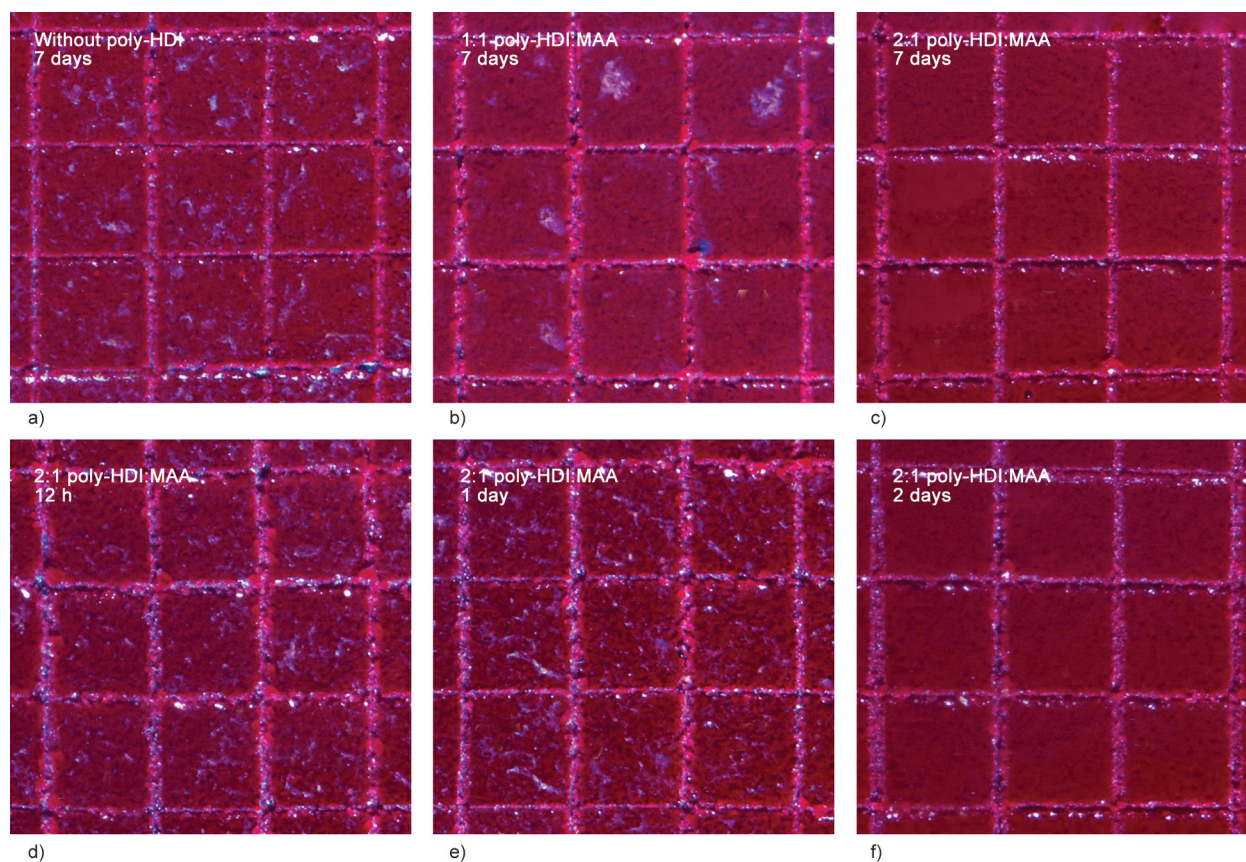


**Figure 6.** Images of steels coated with the NR-g-PMAA primers with the addition of different molar ratios of poly-HDI:MAA after cross-cut testing. a) Without poly-HDI, 7 days, b) 1:1 poly-HDI:MAA, 7 days, c) 2:1 poly-HDI:MAA, 7 days, d) 2:1 poly-HDI:MAA, 12 h, e) 2:1 poly-HDI:MAA, 1 day, f) 2:1 poly-HDI:MAA, 2 days.

classified as a rating of 3B. Note that the cross-cut rating of 5B represented the highest level of adhesion. When the primer was cured using a 1:1 molar ratio of poly-HDI:MAA, the classification of the test results fell within the 3B scale (see Figure 6b). This is because some primer on parts of the square was still detached after the testing. The primer on the steel surface could be classified into 4B level when a poly-HDI:MAA molar ratio of 2:1 was employed. A little detachment of the primer was observed at the intersections of the cuts (see Figure 6c).

The increase in the poly-HDI concentration can improve both the cohesion and adhesion of the primer. The cohesive strength of the primer tends to increase when the NR-g-PMAA chains are chemically linked together by crosslinking. As a result, an increase in the concentration of poly-HDI is expected to improve the primer's cohesive strength. Additionally, poly-HDI can also react with the hydroxyl groups present on the steel surface [9, 10]. Therefore, it can act as a chemical bridge between the primer and the steel surface, increasing adhesion strength. It is important to note that a further increase in the poly-HDI

concentration (*i.e.*, a three-fold molar excess of poly-HDI) had no further effect on the primer's adhesion. From the data, it can be stated that a two-fold molar excess of poly-HDI to MAA is the optimum amount for crosslinking the NR-g-PMAA primer under ambient conditions.

A 7 day cure time was employed to ensure that the primer was completely dried and cured at ambient temperatures. Thus, it is interesting to examine the adhesion rating of the primer with the addition of a 2:1 molar ratio of poly-HDI:MAA at different curing times (ranging from 1 to 7 days). It was observed that the adhesion rating of 3B in the cross-cut test was attained after the primer was allowed to dry at ambient temperatures for 1 day. The curing time required for achieving the cross-cut rating of 4B was about 2 days under ambient conditions, as shown in Figure 6f.

### 3.6. Salt spray test

The salt spray test (SST) has been widely used for accelerated corrosion testing of primer.

In this work, the SST was performed to evaluate the corrosion resistance of the NR-g-PMAA primer with



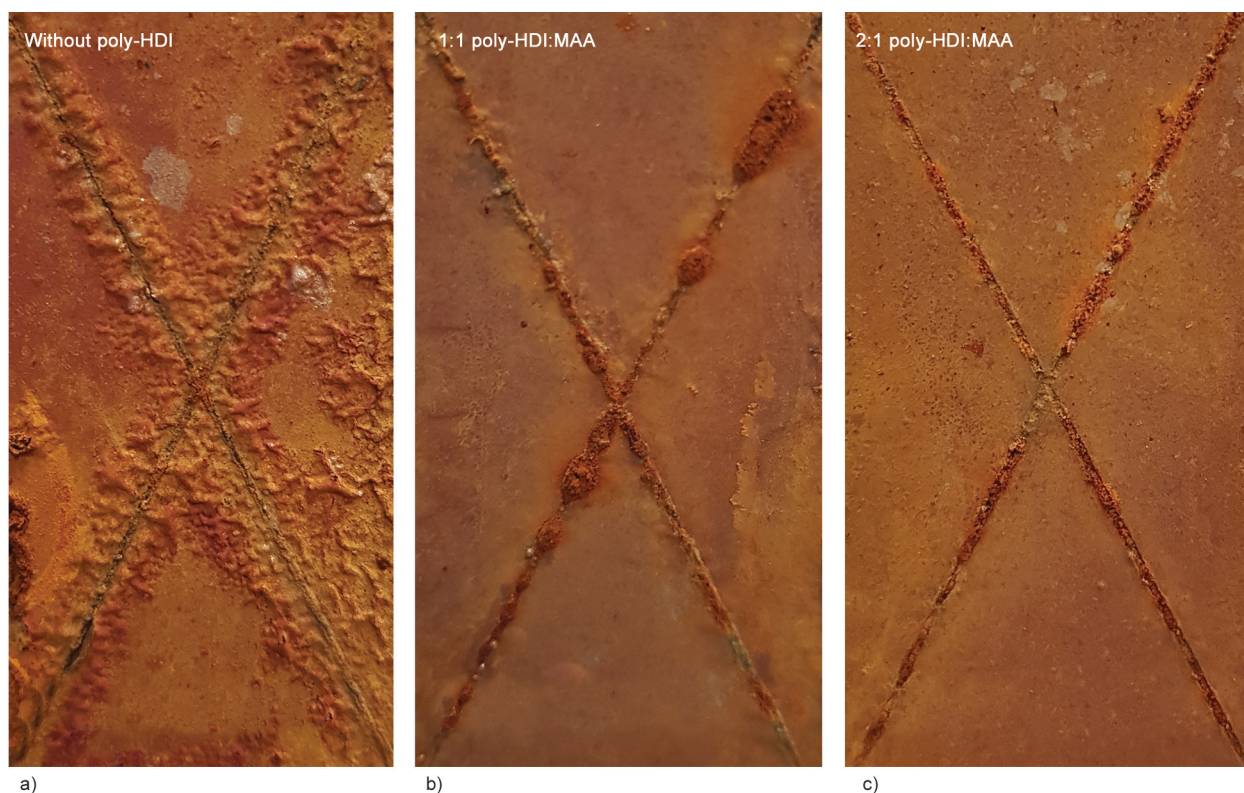


**Figure 7.** Images of steels coated with the NR-g-PMAA primers with the addition of different molar ratios of poly-HDI:MAA after 500 h of the salt spray test. a) Without poly-HDI, b) 1:1 poly-HDI:MAA, c) 2:1 poly-HDI:MAA.

the addition of different molar ratios of poly-HDI:MAA. **Figure 7** reveals that the primer adding a poly-HDI:MAA molar ratio of 2:1 showed no apparent damage outside the scribe lines after the 500 h salt spray testing. However, some rust spots were produced around the scribe lines for the cured primer. It can also be noticed that the rust spots formed after the SST did not collapse upon application of finger pressure, which indicated that they were rust-filled spots. On the other hand, rust deposits were clearly visible on the primer's surface without adding poly-HDI after the salt spray exposure. Corrosion blisters were also observed in areas adjacent to the scribe lines for the uncured primer. These blisters reflected poor interfacial adhesion between the primer and the steel surface, which allowed salt fog to penetrate the underlying steel. Hence, these results demonstrate that incorporating poly-HDI into the primer significantly improved its salt corrosion resistance, resulting from good interfacial adhesion between the primer and steel substrate. Consequently, a 2:1 molar ratio of poly-HDI:MAA was chosen to cure the NR-g-PMAA primer for further study.

### 3.7. QUV-accelerated weathering test

Weathering ageing test of the NR-g-PMAA primers was conducted using a QUV Accelerated Weathering Tester. The surfaces of the steel coated with the NR-g-PMAA primers after 250 and 500 h ageing times are shown in **Figure 8a**.

The result in **Figure 8a** shows that the large rust spots appeared on the steel surface, which had been coated with the uncured primer. It is thought that some cracks would develop in the uncured primer due to degradation when it was exposed to prolonged UV light (*i.e.*, 250 and 500 h). Thus, the steel surface in some areas was left unprotected, allowing the penetration of air and water into the underlying steel. This would accelerate the rusting process during the QUV condensation cycles. In contrast, no traces of rust could be found on the surface of steel coated with the primer with the addition of a 2:1 molar ratio of poly-HDI:MAA. This observation indicated that incorporating poly-HDI into the NR-g-PMAA primer improved its ageing properties.

EDX analysis for the steel surfaces coated with the cured NR-g-PMAA primers is represented in

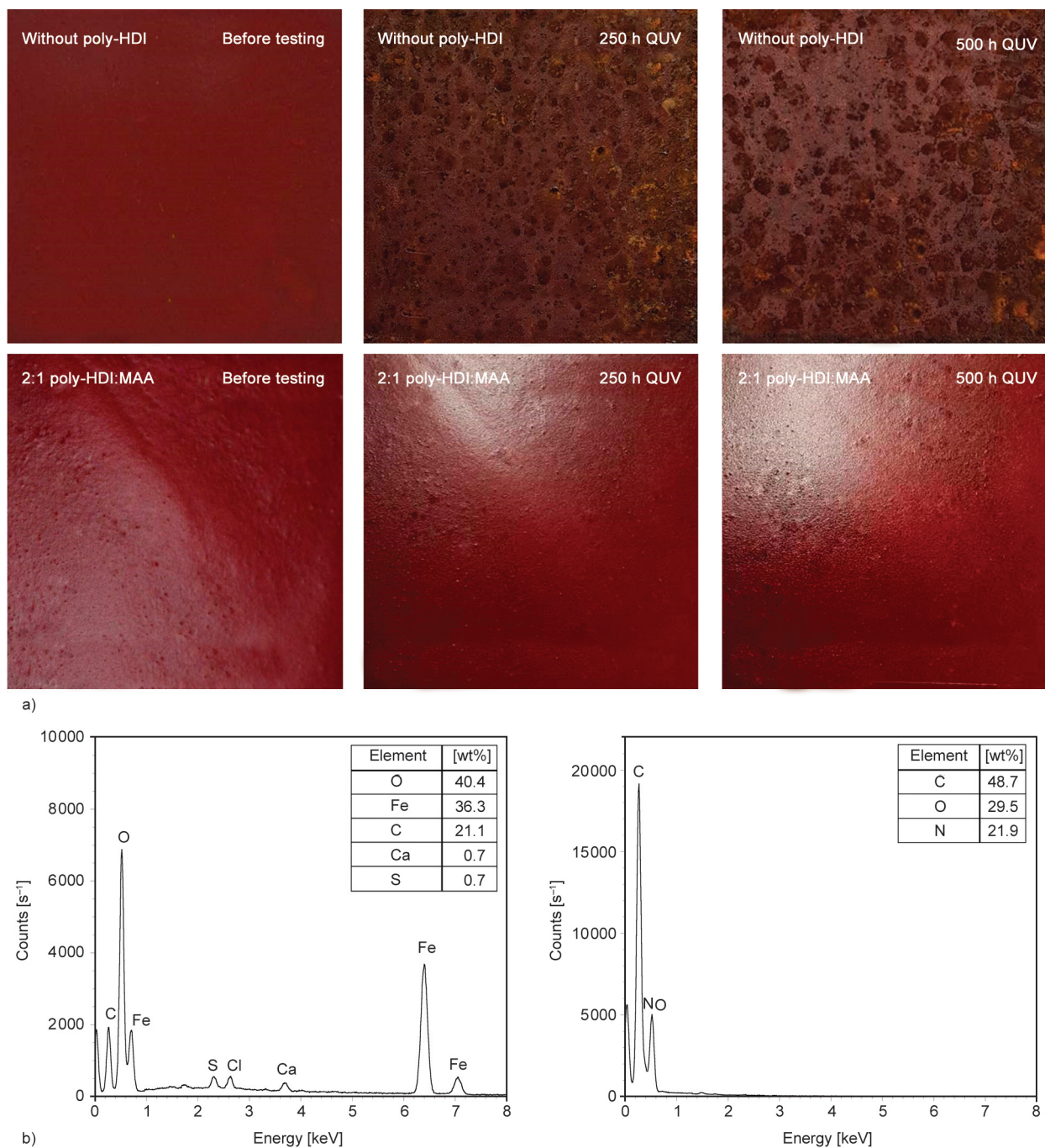


**Figure 8.** (a) The appearance of steels coated with the NR-g-PMAA primer, with or without the addition of poly-HDI, before and after QUV-accelerated weathering aging and (b) EDX surface analysis of the corresponding samples.

**Figure 8b.** It was observed that the surface composition of the corresponding steels consisted mainly of carbon, oxygen, and nitrogen. However, main peaks of Fe element at 6.41 and 7.06 keV were observed in the EDX spectrum of the steel surface coated with the uncured primer [43]. This observation was consistent with the development of rust layers (*i.e.*, iron oxides) on its surface.

Atmospheric corrosion of iron (Fe) is an electrochemical process in which Fe reacts with water and

oxygen through a redox reaction, forming various iron oxides. The primary iron oxides are iron hydroxide ( $\text{Fe}(\text{OH})_2$ ), iron trihydroxide ( $\text{Fe}(\text{OH})_3$ ), goethite ( $\alpha\text{-FeOOH}$ ), akageneite ( $\beta\text{-FeOOH}$ ), lepidocrocite ( $\gamma\text{-FeOOH}$ ), feroxyhyte ( $\delta\text{-FeOOH}$ ), hematite ( $\alpha\text{-Fe}_2\text{O}_3$ ), maghemite ( $\gamma\text{-Fe}_2\text{O}_3$ ), and magnetite ( $\text{Fe}_3\text{O}_4$ ) [44]. These iron oxides have been reported to be present when steel corrodes.

EDX analysis also revealed that oxygen was the primary element (40.4%) present in the steel coated



with the uncured primer after the QUV testing since corrosion products are composed mainly of oxygen and iron. The formation of hydrated iron oxides in the presence of oxygen and water can be shown by the simplified reaction [4] (Equation (11)):



Thus, it can be concluded from these observations that the steel coated with the cured NR-g-PMAA primer was more corrosion resistance than the steel coated with the uncured primer.

### 3.8. Microscopic morphology of the rust layer

The morphologies of the corrosion products formed on rusted weathering steels were also examined using SEM. Figure 9a revealed that large cracks appeared on the surface of the NR-g-PMAA primer without the addition of poly-HDI after 500 h of the QUV weathering test. As a result, corrosion occurred as some areas of the steel surface were exposed to UV light and moisture cycles at elevated temperatures. It was also observed that the morphologies of the oxide layers formed on the weathering steel mainly favored the crystalline globules (sandy crystals) and needle-like shapes.

Although there was no trace of rust on the steel surface coated with the cured NR-g-PMAA primer, micro-crack formation in the primer could be clearly seen in Figure 9a. This is thought to result from the shrinkage and degradation of the NR-g-PMAA primer under accelerated weathering conditions.

The XRD measurement was then performed to study the characteristic structures of crystalline corrosion products. XRD pattern of the corresponding rust layers is shown in Figure 9b. It was found that the primary iron oxides formed in the rust layers were lepidocrocite ( $\gamma$ -FeOOH) and goethite ( $\alpha$ -FeOOH). Lepidocrocite appeared as sandy crystals, which was one of its typical morphological structures [45]. The XRD patterns showed the peaks corresponding to lepidocrocite (L) at 2-theta ( $2\theta$ ) = 14.06, 26.98, 38.00, 46.81, 52.80, and 60.49°. However, lepidocrocite tended to transform into goethite as corrosion proceeded slowly. This is because that goethite is one of the most stable forms of iron oxides [45, 46]. The needle-like morphology in Figure 9a can then be regarded as the structures of goethite formed

on the steel surface after 500 h in a QUV chamber. The characteristic peaks for goethite (G) in the XRD pattern appeared at 21.05, 26.17, 33.08, and 36.50°. Additionally, it was also observed the peaks corresponding to iron (Fe) at 44.63 and 64.00°.

### 4. Conclusions

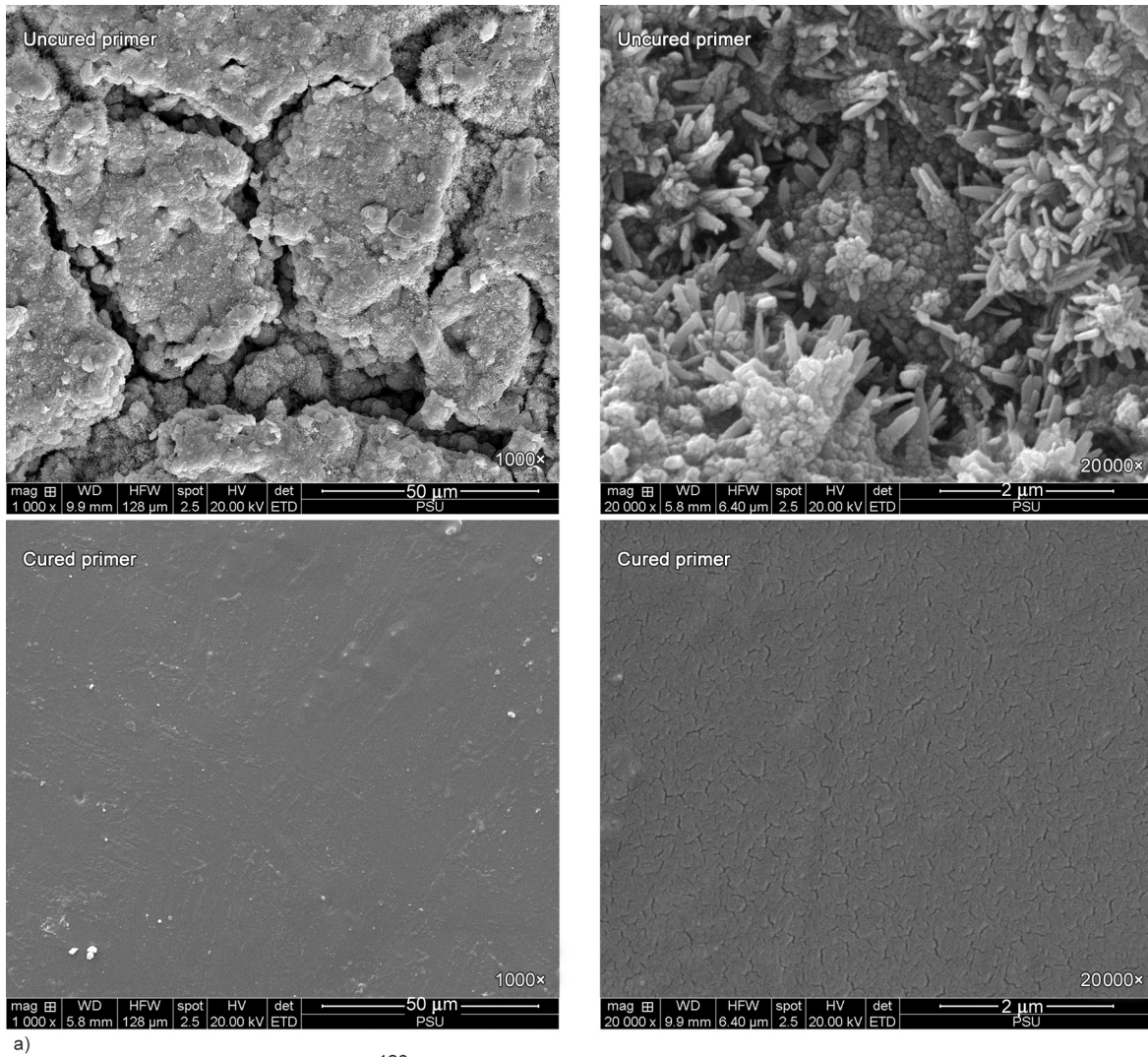
The objective of this study was to develop NR-g-PMAA-based primer for steel. Crosslinking of the NR-g-PMAA primer was achieved by reactions with poly-HDI at room temperature. TGA analysis revealed an increase in the thermal stability of the NR-g-PMAA films by the addition of poly-HDI. Interactions of NR-g-PMAA primer with poly-HDI were investigated by XPS. The results suggest that the crosslinking reaction resulted in the formation of both amide and anhydride linkages. Additionally, XPS analysis also revealed that the poly-HDI could react with the metal hydroxide on the steel surface, leading to a chemical bridge between the primer and the steel substrate.

The salt spray test indicates that the primer provided good adhesion and rust protection to the steel surface when cured using a 2:1 molar ratio of poly-HDI:MAA. This is because no corrosion blisters were present around the edges of the scribe area after the salt spray test. It was also observed that the NR-g-PMAA primer on the steel surface exhibited a 4B class of adhesion as determined by a cross-cut tape test.

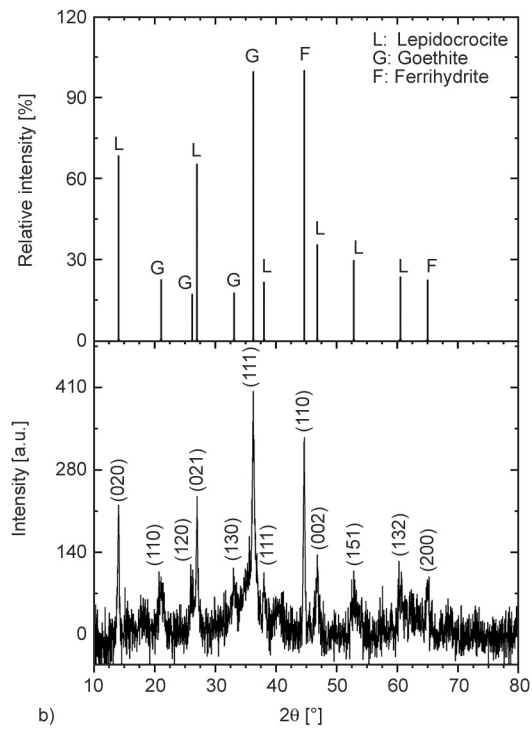
The ability of the corresponding primer to withstand accelerated weathering ageing was also determined using a QUV tester. The result reveals that applying the cured primer on the steel surface could prevent rusting after 500 h artificial QUV weathering. In contrast, the steel coated with the uncured primer was covered with iron oxide deposits (*i.e.*, predominantly lepidocrocite and goethite) after the testing, indicating the degradation of the protective primer layer. Therefore, it can be stated that the NR-g-PMAA has a high potential to develop into an anti-corrosion primer for steel when using poly-HDI as a crosslinker.

### Acknowledgements

This work was supported by the Research Fund of Prince of Songkla University, Pattani Campus, SAT6303037S. The authors also wish to thank BASF (Thai) Ltd. for providing the water dispersible polyisocyanate.



a)



b)

**Figure 9.** (a) SEM images of steels coated with the NR-g-PMAA primer, with or without the addition of poly-HDI after 500 h of exposure in a QUV chamber and (b) XRD analysis of rust layers formed on the steel surface.



## References

- [1] Ebnesajjad S.: Adhesives technology handbook. William Andrew, Norwich (2009).
- [2] Kuhn L. B.: Rubber to metal adhesive comprising dichlorobutadiene resin and a chlorinated elastomer and use thereof. U.S. Patent 2581920A, USA (1952).
- [3] Halladay J. R., Warren P. A.: Rubber to metal bonding. in 'The handbook of rubber bonding' (ed.: Crowther B.) Rapra, Shawbury, 57–80 (2003).
- [4] Sørensen P. A., Kiil S., Dam-Johansen K., Weinell C. E.: Anticorrosive coatings: A review. *Journal of Coatings Technology and Research*, **6**, 135–176 (2009).  
<https://doi.org/10.1007/s11998-008-9144-2>
- [5] Bhowmick A. K., Hall M. M., Benarey H. A.: Rubber products manufacturing technology. Marcel Dekker, New York (1994).
- [6] Schollenberger C. S.: Polyurethane- and isocyanate-based adhesives. in 'Handbook of adhesives' (ed.: Skeist I.) Springer, Boston, 359–380 (1990).  
[https://doi.org/10.1007/978-1-4613-0671-9\\_20](https://doi.org/10.1007/978-1-4613-0671-9_20)
- [7] Achary P. S., Gouri C., Ramaswamy R.: Reactive bonding of natural rubber to metal by a nitrile-phenolic adhesive. *Journal of Applied Polymer Science*, **81**, 2597–2608 (2001).  
<https://doi.org/10.1002/app.1702>
- [8] Mowrey D. H., Carney B. P., Cowles R. S., Agag T.: Adhesive composition and method for bonding. U.S. Patent 20180244965A1, USA (2018).
- [9] Shimizu K., Phanopoulos C., Loenders R., Abel M. L., Watts J. F.: The characterization of the interfacial interaction between polymeric methylene diphenyl diisocyanate and aluminum: A ToF–SIMS and XPS study. *Surface and Interface Analysis*, **42**, 1432–1444 (2010).  
<https://doi.org/10.1002/sia.3586>
- [10] Tardio S., Abel M-L., Carr R. H., Watts J. F.: The interfacial interaction between isocyanate and stainless steel. *International Journal of Adhesion and Adhesives*, **88**, 1–10 (2019).  
<https://doi.org/10.1016/j.ijadhadh.2018.10.008>
- [11] van Amerongen G. J., Koningsberger C.: Chlorination of natural rubber. II. Preparation and properties of rubber dichloride. *Journal of Polymer Science*, **5**, 653–666 (1950).  
<https://doi.org/10.1002/pol.1950.120050602>
- [12] Zhong J-P., Li S-D., Wei Y-C., Peng Z., Yu H-P.: Study on preparation of chlorinated natural rubber from latex and its thermal stability. *Journal of Applied Polymer Science*, **73**, 2863–2867 (1999).  
[https://doi.org/10.1002/\(SICI\)1097-4628\(19990929\)73:14<2863::AID-APP9>3.0.CO;2-2](https://doi.org/10.1002/(SICI)1097-4628(19990929)73:14<2863::AID-APP9>3.0.CO;2-2)
- [13] Rawlings E. G.: Corrosion-resistant coatings: Natural, chlorinated and synthetic rubber. *Anti-Corrosion Methods and Materials*, **4**, 283–286 (1957).  
<https://doi.org/10.1108/eb019370>
- [14] Sakhri A., Perrin F. X., Aragon E., Lamouric S., Benaboura A.: Chlorinated rubber paints for corrosion prevention of mild steel: A comparison between zinc phosphate and polyaniline pigments. *Corrosion Science*, **52**, 901–909 (2010).  
<https://doi.org/10.1016/j.corsci.2009.11.010>
- [15] Mousaa I., Radi H.: New corrosion inhibitors based on epoxidized natural rubber for coating protection of metals under UV irradiation. *Anti-Corrosion Methods and Materials*, **64**, 389–396 (2017).  
<https://doi.org/10.1108/ACMM-01-2016-1628>
- [16] Ninjan R., Thongnuanchan B., Lopattananon N., Thitithammawong A., Nakason C.: Rubber-to-steel adhesives based on natural rubber grafted with poly(acetoacetoxyethyl methacrylate). *Journal of Polymer Engineering*, **41**, 192–201 (2021).  
<https://doi.org/10.1515/polyeng-2020-0156>
- [17] Nontasak W., Thongnuanchan B., Ninjan R., Lopattananon N., Wannavilai P., Nakason C.: Fire-retardant wood coating based on natural rubber bearing methacrylic functionality. *Journal of Polymer Engineering*, **41**, 44–53 (2021).  
<https://doi.org/10.1515/polyeng-2020-0092>
- [18] Thongnuanchan B., Ninjan R., Kaesaman A., Nakason C.: Synthesis of modified natural rubber with grafted poly(acetoacetoxyethyl methacrylate-co-methyl methacrylate) and performance of derived adhesives with GTA crosslinker. *Polymer Engineering and Science*, **58**, 1610–1618 (2018).  
<https://doi.org/10.1002/pen.24750>
- [19] Wu S.: Calculation of interfacial tension in polymer systems. *Journal of Polymer Science Part C: Polymer Symposia*, **34**, 19–30 (1971).  
<https://doi.org/10.1002/polc.5070340105>
- [20] Wu S.: Polymer interface and adhesion. Marcel Dekker, New York (1982).
- [21] Ellis B., Welding G. N.: Estimation, from swelling, of the structural contribution of chemical reactions to the vulcanization of natural rubber. Part I. General method. *Rubber Chemistry and Technology*, **37**, 563–570 (1964).  
<https://doi.org/10.5254/1.3540348>
- [22] Flory P. J., Rehner J.: Statistical mechanics of cross-linked polymer networks II. Swelling. *The Journal of Chemical Physics*, **11**, 521–526 (1943).  
<https://doi.org/10.1063/1.1723792>
- [23] Valentín J. L., Carretero-González J., Mora-Barrantes I., Chassé W., Saalwächter K.: Uncertainties in the determination of cross-link density by equilibrium swelling experiments in natural rubber. *Macromolecules*, **41**, 4717–4729 (2008).  
<https://doi.org/10.1021/ma8005087>
- [24] Chassé W., Lang M., Sommer J-U., Saalwächter K.: Cross-link density estimation of PDMS networks with precise consideration of networks defects. *Macromolecules*, **45**, 899–912 (2012).  
<https://doi.org/10.1021/ma202030z>

- [25] Yusof N. H., Kosugi K., Song T. K., Kawahara S.: Preparation and characterization of poly(stearyl methacrylate) grafted natural rubber in latex stage. *Polymer*, **88**, 43–51 (2016).  
<https://doi.org/10.1016/j.polymer.2016.02.005>
- [26] Vuckovac M., Latikka M., Liu K., Huhtamäki T., Ras R. H. A.: Uncertainties in contact angle goniometry. *Soft Matter*, **15**, 7089–7096 (2019).  
<https://doi.org/10.1039/C9SM01221D>
- [27] von Fraunhofer J. A.: Adhesion and cohesion. *International Journal of Dentistry*, **3**, 951324 (2012).  
<https://doi.org/10.1155/2012/951324>
- [28] Wenzel R. N.: Resistance of solid surfaces to wetting by water. *Industrial and Engineering Chemistry*, **28**, 988–994 (1936).  
<https://doi.org/10.1021/ie50320a024>
- [29] Packham D. E.: Surface energy, surface topography and adhesion. *International Journal of Adhesion and Adhesives*, **23**, 437–448 (2003).  
[https://doi.org/10.1016/S0143-7496\(03\)00068-X](https://doi.org/10.1016/S0143-7496(03)00068-X)
- [30] Cassie A. B. D.: Contact angles. *Discussions of the Faraday Society*, **3**, 11–16 (1948).  
<https://doi.org/10.1039/dF9480300011>
- [31] Schotman A. H. M., Mijs W. J.: Carbodiimides as important intermediates in the reaction of isocyanates with carboxylic acids. *Recueil des Travaux Chimiques des Pays-Bas*, **111**, 88–91 (1992).  
<https://doi.org/10.1002/recl.19921110205>
- [32] Ninjan R., Thongnuanchan B., Lopattananon N., Thitithammawong A., Nakason C.: Ambient curable latex films and adhesives based on natural rubber bearing acetoacetoxy functionality. *Polymers for Advanced Technologies*, **30**, 598–607 (2019).  
<https://doi.org/10.1002/pat.4496>
- [33] Lin S.-Y., Cheng W.-T., Wei Y.-S., Lin H.-L.: DSC-FTIR microspectroscopy used to investigate the heat-induced intramolecular cyclic anhydride formation between Eudragit E and PVA copolymer. *Polymer Journal*, **43**, 577–580 (2011).  
<https://doi.org/10.1038/pj.2011.15>
- [34] Wang P., Tan K. L., Ho C. C., Khew M. C., Kang E. T.: Surface modification of natural rubber latex films by graft copolymerization. *European Polymer Journal*, **36**, 1323–1331 (2000).  
[https://doi.org/10.1016/S0014-3057\(99\)00193-7](https://doi.org/10.1016/S0014-3057(99)00193-7)
- [35] Haverkamp R. G., Siew D. C. W., Barton T. F.: XPS study of the changes during the service life of polyester powder coatings. *Surface and Interface Analysis*, **33**, 330–334 (2002).  
<https://doi.org/10.1002/sia.1215>
- [36] Ederer J., Janoš P., Ecorchard P., Tolasz J., Štengl V., Beneš H., Perchacz M., Pop-Georgievski O.: Determination of amino groups on functionalized graphene oxide for polyurethane nanomaterials: XPS quantitation vs. functional speciation. *Royal Society of Chemistry*, **7**, 12464–12473 (2017).  
<https://doi.org/10.1039/C6RA28745J>
- [37] Jansen R. J. J., van Bekkum H.: XPS of nitrogen-containing functional groups on activated carbon. *Carbon*, **33**, 1021–1027 (1995).  
[https://doi.org/10.1016/0008-6223\(95\)00030-H](https://doi.org/10.1016/0008-6223(95)00030-H)
- [38] Grant D. H., Grassie N.: The thermal decomposition of poly(*t*-butyl methacrylate). *Polymer*, **1**, 445–455 (1960).  
[https://doi.org/10.1016/0032-3861\(60\)90060-4](https://doi.org/10.1016/0032-3861(60)90060-4)
- [39] McNeill I. C., Ligga J. J.: Thermal degradation of styrene-methacrylic acid copolymers. *Polymer Degradation and Stability*, **36**, 291–299 (1992).  
[https://doi.org/10.1016/0141-3910\(92\)90069-H](https://doi.org/10.1016/0141-3910(92)90069-H)
- [40] Menon A. R. R., Pillai K. S., Nando G. B.: Thermal degradation characteristics of natural rubber vulcanizates modified with phosphorylated cashew nut shell liquid. *Polymer Degradation and Stability*, **52**, 265–271 (1996).  
[https://doi.org/10.1016/0141-3910\(96\)00007-9](https://doi.org/10.1016/0141-3910(96)00007-9)
- [41] Lai J. H.: Thermal behavior of random copolymers of methacrylic acid and *tert*-butyl methacrylate. *Macromolecules*, **17**, 1010–1012 (1984).  
<https://doi.org/10.1021/ma00135a006>
- [42] Cárdenas G., Muñoz C., Carbacho H.: Thermal properties and TGA-FTIR studies of polyacrylic and poly-methacrylic acid doped with metal clusters. *European Polymer Journal*, **36**, 1091–1099 (2000).  
[https://doi.org/10.1016/S0014-3057\(99\)00187-1](https://doi.org/10.1016/S0014-3057(99)00187-1)
- [43] Yu J., Ji G., Liu Q., Zhang J., Shi Z.: Effect of sol-gel ZrO<sub>2</sub> films on corrosion behavior of the 304 stainless steel in coal-gases environment at high temperature. *Surface and Coatings Technology*, **331**, 21–26 (2017).  
<https://doi.org/10.1016/j.surfcoat.2017.10.037>
- [44] Oh Sei J., Cook D. C., Townsend H. E.: Characterization of iron oxides commonly formed as corrosion products on steel. *Hyperfine Interactions*, **112**, 59–66 (1998).  
<https://doi.org/10.1023/A:1011076308501>
- [45] Fonna S., Ibrahim I. B. M., Gunawarman, Huzni S., Ikhsan M., Thalib S.: Investigation of corrosion products formed on the surface of carbon steel exposed in Banda Aceh's atmosphere. *Heliyon*, **7**, e06608 (2021).  
<https://doi.org/10.1016/j.heliyon.2021.e06608>
- [46] Misawa T., Hashimoto K., Shimodaira S.: The mechanism of formation of iron oxide and oxyhydroxides in aqueous solutions at room temperature. *Corrosion Science*, **14**, 131–149 (1974).  
[https://doi.org/10.1016/S0010-938X\(74\)80051-X](https://doi.org/10.1016/S0010-938X(74)80051-X)